Pharm Res (2012) 29:546–558
DOI 10.1007/s11095-011-0641-0

RESEARCH PAPER

Nose-to-Brain Transport Pathways of Wheat Germ Agglutinin Conjugated PEG-PLA Nanoparticles

Qingfeng Liu • Yehong Shen • Jie Chen • Xiaoling Gao • Chengcheng Feng • Lu Wang • Qizhi Zhang • Xinguo Jiang

Received: 18 July 2011 / Accepted: 4 December 2011 / Published online: 14 December 2011

ABSTRACT

Purpose To investigate the possible pathways for transport of wheat germ agglutinin conjugated PEG-PLA nanoparticles (WGA-NP) into the brain after nasal administration.

Methods The nose-to-brain pathways were investigated using WGA-NP containing 6-coumarin (as a fluorescent marker) and ^{125}I-labeled WGA-NP. *Ex vivo* imaging analysis was also employed to visualize the transport process.

Results Nasal administration of WGA-NP to rats resulted in transcellular absorption across the olfactory epithelium and transfer to the olfactory bulb within 5 min. After entering the lamina propria, a proportion of WGA-NP were transferred from the olfactory nerve bundles and their surrounding connective tissue to the olfactory bulb. The trigeminal nerves also contributed to WGA-NP brain transfer, especially to WGA-NP distribution in the caudal brain areas. However, cerebrospinal fluid pathway may have little contribution to the process of transferring WGA-NP into the central nervous system (CNS) after intranasal administration.

Conclusions These results demonstrated that intranasally administered WGA-NP reach the CNS via olfactory pathway and trigeminal nerve pathway, and extracellular transport along these nerves is the most possible mechanism.

Q. Liu • Y. Shen • J. Chen • C. Feng • L. Wang • Q. Zhang (✉) • X. Jiang
Department of Pharmaceutics, School of Pharmacy, Fudan University
826 Zhangheng Road, Room 604
Shanghai 201203, People's Republic of China
e-mail: qzzhang70@yahoo.com.cn

Q. Liu • Y. Shen • J. Chen • C. Feng • L. Wang • Q. Zhang • X. Jiang
Key Laboratory of Smart Drug Delivery, Ministry of Education & PLA
Shanghai, People's Republic of China 201203

X. Gao
Department of Pharmacology, College of Basic Medical Sciences
Shanghai Jiao Tong University
Shanghai 200025, People's Republic of China

KEY WORDS CNS · nasal route · olfactory pathway · trigeminal nerve pathway. · WGA-NP

INTRODUCTION

As a convenient and efficient method transporting drugs or their carriers to the brain, intranasal delivery has attracted more and more attention in the past decade (1). After intranasal administration, drugs can directly reach the central nervous system (CNS) for treatment of CNS diseases via nose-to-brain pathways, minimizing systemic exposure and decreasing side effects (2). However, for macromolecules such as peptides, proteins and nucleic acids, easy clearance or degradation in the nasal cavity leads to their very low transport efficiency to the brain (3,4).

In our previous work, intranasal administration of vasoactive intestinal peptide (VIP; M_W 3326) incorporated in wheat germ agglutinin (WGA) conjugated PEG-PLA nanoparticles (WGA-NP) has been demonstrated to be a promising method for protecting peptides from peptidase degradation and enhancing transport of peptides to the CNS (5). The bioavailability of intact VIP in mice brain following intranasal instillation of VIP-loaded WGA-NP was significantly increased by 5.6~7.7 folds and 1.58~1.82 folds, compared with intranasal solution and unmodified nanoparticles, respectively. The increase of VIP concentration in brain also contributed to the improved memory function of ethylcholine aziridium-treated rats, as demonstrated by the Morris water maze test (5). These intriguing results clearly proved WGA-NP to be a suitable carrier for intranasal delivery of macromolecules such as peptides and proteins. However, the pathways of nanoparticles transferring into the CNS following nasal administration remain unclear.

Mathison *et al.* (6) summarized two pathways for direct delivery of solutes from the nasal cavity to the brain: 1) olfactory nerve pathway: solutes may enter the brain by moving into the olfactory dendrites and be propelled by axonal flow to the olfactory bulb; 2) olfactory epithelial pathway: solutes may permeate the nasal epithelium by way of pinocytosis, diffusion or paracellular transport, followed by transfer in the perineural space around the olfactory nerve bundles to the CSF surrounding the brain. The two pathways are collectively called olfactory pathway, which have been confirmed by many studies. For example, Prussian blue was used to visualize the olfactory pathways after intranasal administration to rabbits and mice (7,8). The dye was observed in the olfactory mucosa and the perineural sheaths of the olfactory nerve, indicating that absorption across the epithelium was mainly associated with the olfactory cells (8). Jansson and Bjork (9) visualized the distribution of a 3 kDa fluorescein dextran (FD3) in the olfactory epithelium, the respiratory epithelium, the submucosa, the cribriform plate region and the olfactory bulb following nasal administration to rats using fluorescence microscopy. They found that FD3 was absorbed across the olfactory epithelium mainly via a transcellular way and then quickly transported to the olfactory bulb along the olfactory nerve bundles. In the last few years, intranasal drug delivery along another pathway- trigeminal nerve pathway was demonstrated (10,11). Throne *et al.* (10) found that about 10 folds higher radioactivity was detected in the trigeminal nerve branches than that in the olfactory bulb after intranasal administration of ^{125}I-IGF-I. Since the trigeminal nerve widely innervates the respiratory and olfactory epithelium and enters the brain stem in the pons (1), it is important to note the trigeminal-mediated transport of intranasally administered drugs to the CNS, especially in brain areas distant from the olfactory bulb.

Previous studies of transport mechanisms in the nasal cavity have focused on viruses, dye, metals, macromolecules such as FD3 and WGA conjugated horseradish peroxidase (12). However, little is known about the mechanisms of direct transport of nanoparticles into the brain. To improve the application of WGA-NP in nasal drug delivery in practice, exploring the possible pathways that nanoparticles can follow after nasal administration is necessary. In this study, the widely used lipophilic 6-coumarin was encapsulated into the nanoparticles (13,14) and used for visualizing the localization of nanoparticles in the nasal cavity and olfactory bulb by fluorescence microscopy, combined with immunohistochemistry dyeing to determine 1) whether WGA-NP has higher affinity to olfactory epithelium; 2) absorption pathways of WGA-NP through the epithelium; 3) whether WGA-NP are transferred to olfactory bulb along nerve bundles. Also, WGA-NP were radiolabelled with ^{125}I, and the levels of radioactivity in blood, lymph nodes, trigeminal nerve, CSF and brain tissues were measured after intranasal instillation of ^{125}I-WGA-NP to Sprague–Dawley rats, to determine the pathways of WGA-NP transport into the brain. Moreover, *ex vivo* imaging technology was employed to visualize the brain transfer of NP and WGA-NP after intranasal administration.

MATERIALS AND METHODS

Materials

Maleimide- poly(ethylene glycol)$_{3000}$-poly(lactic acid)$_{70000}$ (Male-PEG-PLA) and methoxy poly(ethylene glycol)$_{3000}$-poly(lactic acid)$_{50000}$ (MePEG-PLA) were kindly gifted by East China University of Science. WGA was purchased from Vector Laboratories (UK); 2-iminothiolane and 4′,6-diamidino-2-phenylindole (DAPI) from Sigma; 6-coumarin from Aldrich; 1,1′-dioctadecyl-3,3,3′,3′-tetramethyl indotricarbocyanine Iodide (DiR) from Biotium (USA). Rabbit anti-rat Zonula Occludens Protein 1 (ZO-1) antibody was supplied by Santa Cruz (USA); Rabbit anti-nerve specific enolase (NSE) polyclonal antibody and Cy3-conjugated goat anti-rabbit IgG were obtained from Wuhan Boster Biological Technology Ltd. All the other reagents were of HPLC or analytical grade.

Male Sprague–Dawley (SD) rats (200–220 g) were purchased from Sino-British Sippr/BK Lab Animal Ltd. (Shanghai, China) and housed in accordance with the guidelines of the "Principles of Laboratory Animal Care" (NIH publication #85-23, revised in 1985).

Preparation of Fluorescent Probe-Loaded WGA Conjugated PEG-PLA Nanoparticles

PEG-PLA nanoparticles (NP) were prepared by the emulsion/solvent evaporation method (14). Briefly, MePEG-PLA (22.5 mg), Male-PEG-PLA (2.5 mg) and 6-coumarin (1 mg) were dissolved in 1 ml of dichloromethane and added into 2 ml of 1% sodium cholate, followed by emulsion at 280 w for 1 min using a probe sonicator (Scientz Biotechnology Co. Ltd., China) in ice bath. The o/w emulsion was then dispersed in 25 ml of 0.5% sodium cholate and magnetically stirred for 5 min. After dichloromethane evaporation, the nanoparticles were concentrated by centrifugation (21,000 g×45 min) and the unentrapped 6-coumarin was removed using a 1.5×20 cm sepharose CL-4B column with 0.05 M HEPES buffer (pH 7.0) adding 0.15 M NaCl as the eluent. DiR-loaded nanoparticles, used for *ex vivo* imaging, were prepared with the same procedure except that 0.05% (w/v)

of DiR was added to the dichloromethane solution before emulsification.

The NPs reacted with 2-iminothiolane thiolated WGA at room temperature for 8 h at a molar ratio of WGA: maleimide of 1:10. WGA-NP were separated from unconjugated WGA by centrifugation at 21,000×g for 45 min and washing with phosphate buffered saline (PBS).

Particle size of nanoparticles was measured by dynamic light scattering using a Nicomp^{TM} 380 XLS Zeta Potential/ Particle Sizer (PSS·Nicomp, USA). *In vitro* release of 6-coumarin or DiR-loaded nanoparticles was conducted in PBS (pH 4.0 and pH 7.4) at 37°C. DiR was determined by spectrophotometry using a UV-2401 spectrophotometer (Shimadzu, Japan) at 670 nm and 6-coumarin was determined by high performance liquid chromatography as described before (14).

The resulting nanoparticles encapsulating 6-coumarin had a mean diameter of 110 nm, with an encapsulation efficiency of about 70%. DiR-loaded nanoparticles (DiR-NP) and modified nanoparticles (WGA-DiR-NP) had a mean diameter of 95 and 112 nm, respectively. *In vitro* release study of nanoparticles showed that lower than 2% of 6-coumarin and 4% of DiR were released from nanoparticles, after an 8-h incubation period. Therefore, the fluorescence observed in the nasal cavity and brain within 2 h after intranasal administration was mainly due to the uptake of nanoparticles, not free dye. Besides, the fluorescence signals of 6-coumarin and DiR remained consistent at 37°C within 8 h.

Transport Visualization of 6-Coumarin-Loaded WGA-NP

In order to visualize the distribution of WGA-NP in the nasal mucosa and olfactory bulb, SD rats under anesthetization with 5% chloral hydrate were placed in a supine position and given intranasally with 50 μl of 6-coumarin-loaded WGA-NP (5 mg/kg) (into the right nostril) via a polyethylene tube attached to the top of a microsyringe. At each time point (5, 30 and 120 min) after administration, 2–3 rats were perfused with physiological saline and 4% paraformaldehyde. The right nasal cavity and olfactory bulb were isolated and fixed for 24 h.

The nasal cavity was decalcified and cut into four slices with a 2–3 mm thickness according to a previously reported schedule (9) (Fig. 1 top). After dehydration in sucrose solution, the slices were embedded in Tissue-Tek® O.C.T compound (Sakura Finetek, USA) and cut (5 μm) on a Leica 5a microtome (Leica, Germany). The olfactory bulb was dehydrated, embedded and sectioned (10 μm) directly with the same procedure as above. Counterstained with DAPI (1 μg/ml), the sections were examined using an Olympus IX71 fluorescence microscope (Japan).

The olfactory mucosa and olfactory nerve bundles were characterized by immunohistochemistry staining with anti-nerve specific enolase (NSE) as the primary antibody, as reported previously (15). Briefly, the sections were placed in normal goat serum for 20 min and treated with 1:200 rabbit anti-NSE monoclonal antibody at 37°C for 30 min and at 4°C for 12 h. After washing with PBS, the sections were incubated with 1:400 Cy3-conjugated goat-anti-rabbit IgG. Following counterstaining with DAPI, the sections were observed under an Olympus IX71 fluorescence microscope. The tight junction was also stained by the same procedure as above except that the first antibody was ZO-1 antibody at 1:150 dilution.

Distribution of WGA-NP in the Brain

WGA-NP Radiolabelling and Purification

WGA-NP were radioiodinated according to the iodogen methods as described by Qian *et al.* (16). Briefly, 60 μl of WGA-NP solution (about 15 μg of WGA) was incubated for 5 min at 30°C with 3.09 mCi of $Na^{125}I$ in PBS (pH 7.4, 0.1 M) in an iodogen®-coated tube (iodogen®: 1,3,4,6-tetrachloro-3,6-diphenylglycoluril, Chengdu Gaotong Isotope Corporation, China), and then ^{125}I-WGA-NP were separated with a Sephadex G-25 (0.5 mm×10 mm) column. The purified ^{125}I-WGA-NP were further concentrated by Centricon-3 devices (3 K, Millipore, USA) and analyzed for radioactivity in an SN-682 Gamma ratioimmunoassay counter (Ri Huan Instrument Factory of Shanghai, China). The labelling efficiency of resulting nanoparticles was 67% and radiochemical purity was 95%.

Stability of ^{125}I-WGA-NP in Brain Homogenate

Since ^{125}I labeled on the protein will fall off with the prolongation of storage and enzyme effect *in vivo* (17), the stability of ^{125}I-WGA-NP in brain homogenate was investigated in this study. Nanoparticles were dispersed in fresh rat brain homogenate (1:9 in PBS) at a radioactivity of about 100 μCi. The samples were incubated at 37°C with a rotating rate of 100 r/min. Samples (n=3) were withdrawn at predetermined time and subjected to centrifugation at 21,000 g for 1 h and the supernatant was then γ-counted. In order to compensate the influence of time-related decay of ^{125}I, three additional samples were simultaneously taken for the determination of the total amount of radioactivity retained in the samples at each time point. The percentage of intact ^{125}I-WGA-NP retained was calculated as follow:

$$^{125}I-WGA-NP\% = \frac{cpm_{T,t} - cpm_{S,t}}{cpm_{T,t}} \times 100\%$$

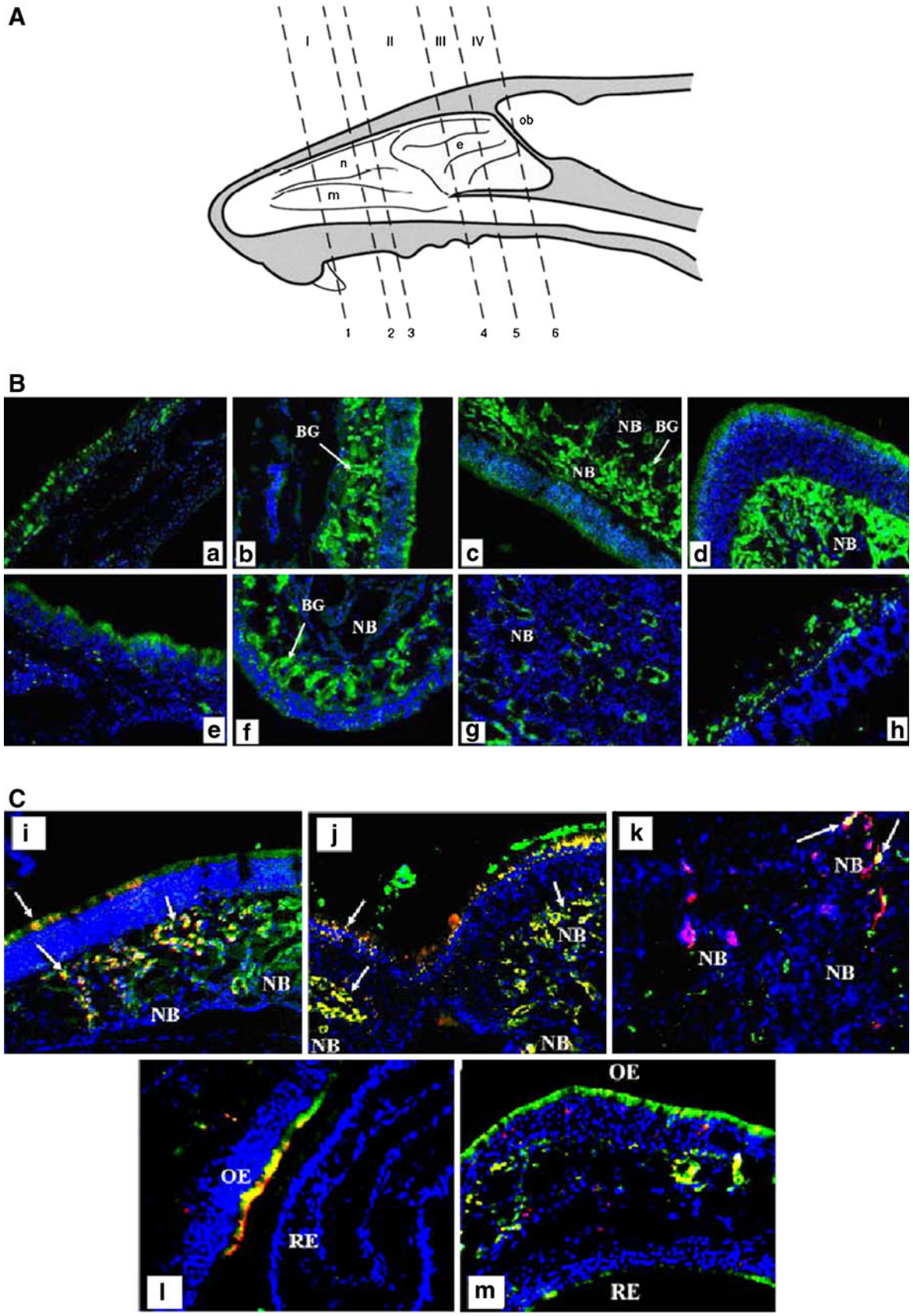
A
I
II
III
IV
ob
e
n
m
1
2
3
4
5
6
B
BG
NB
a
b
c
d
e
f
g
h
C
i
j
k
l
m
OE
RE

◀ **Fig. 1** (**A**) Four nasal slices (levels I, II, III, and IV) were made according to the report by Jansson and Bjork (9). The symbols I-IV denote the various slices obtained. (**B**) Distribution of WGA-NP (*green*) in slices I (**a**,**e**), II (**b**,**f**), III (**c**,**g**), IV (**d**,**h**) of nasal cavity 30 min after intranasal administration of coumarin-6-loaded WGA-NP to rats at a dose of 5 mg/kg. Cell nucleus stained with DAPI (*blue*). (**C**) Distribution of WGA-NP in slices III (**I**) and IV (**j**, **k**) 30 min following intranasal administration. WGA-NP exhibited higher affinity to the olfactory mucosa than that to the respiratory one (**l**, **m**). Olfactory receptor cells and nerve bundles positive stained (*red*) and cell nucleus stained with DAPI (blue). e: ethmoid turbinates, m: maxilloturbinate, n: nasoturbinate, ob: olfactory bulb. OE: olfactory epithelium, RE: respiratory epithelium, BG: Bowman gland, NB: nerve bundle, and co-locations (*yellow*) of the green and red fluorescence are shown by arrows. (200×).

Where ^{125}I-WGA-NP% represents the percentage of intact ^{125}I-WGA-NP retained in brain, $cpm_{T,t}$ and $cpm_{S,t}$ stand for the total radioactivity and the radioactivity in supernatant at t time point, respectively.

After incubation with rat brain homogenate for 2 and 4 h, about 91.11±6.65% and 90.43±3.21% specific activity were from ^{125}I-WGA-NP, respectively, indicating the deiodination of labeled nanoparticles was not obvious within 2 h. Therefore, the radioactivity measured in the rat brain tissues mainly originated from intact nanoparticles but not free iodine or nanoparticle fragments.

Animal Experiment

SD rats were anesthetized and given 20 μl (about 50 μCi) of ^{125}I-WGA-NP suspension in PBS (25 mg/ml) into the right nostril. At 5, 30 and 120 min after administration, CSF samples (about 50 μl) were withdrawn by cisternal puncture (18). Then blood was sampled from the heart and animals were heart-perfused with ice-cold saline. After that, the superficial and deep cervical lymph nodes as well as the axillary lymph nodes were isolated. The brain was separated and microdissected with a scalpel carefully. The trigeminal nerves were isolated from bone tissue of skull base and dissected from the root of trigeminal nerve to the anterior lacerated foramen and the foramen ovale (10). Sample were weighted and subjected to gamma counting. The amount of ^{125}I-WGA-NP in tissues was expressed as the percentage of the radioactivity in tissues accounting for the administration dose and calculated according to the following equation. For each time point six animals were applied.

$$\text{Amount of } {}^{125}\text{I} - \text{WGA} - \text{NP in the tissues (\%)} = \frac{\text{radioactivity counts per gram tissue}}{\text{dose per gram body weight}} \times 100\%$$

Ex Vivo Imaging of DiR-Loaded NP and WGA-NP

SD rats were anesthetized and given intranasally 50 μl (25 μl/nostril) of DiR-NP and WGA-DiR-NP at a dose of 10 mg/kg. At 5, 30 and 120 min post administration, the rats were anesthetized and perfused with physiological saline. The brain, olfactory bulb and trigeminal nerve of the rats were carefully isolated and visualized by CRi *in vivo* imaging system (MA, USA). After that, the brains were subjected to sagittal slicing and the 3-mm midsagittal sections were observed. Measurements were made on three rats at each time point.

RESULTS AND DISCUSSION

Transport Visualization of 6-Coumarin-Loaded WGA-NP

Distribution of WGA-NP in Rat Nasal Mucosa

In order to obtain direct evidence about the olfactory transfer of WGA-NP, 6-coumarin (emitting green fluorescence) loaded nanoparticles were given intranasally to rats. DAPI, a nucleus-specific dye that emits blue fluorescence, was used to detect cell localization. Since olfactory cells are the only sensory neurons with their cell bodies in the nose epithelia, NSE positive staining epithelia (red) in Fig. 1 bottom were considered as olfactory epithelia.

WGA-NP were uptaken rapidly and strong green fluorescence signals were observed at 5 and 30 min after administration, with comparable intensity between the two time points. After 2 h, the fluorescence intensity decreased slightly. Figure 1 middle shows the distribution of WGA-NP in four levels (as defined in Fig. 1 top) of rat nasal cavity 30 min after administration. WGA-NP distributed mainly in epithelia in level I (Fig. 1a, e) with relatively strong fluorescence signals observed in the ciliated cells. A few nanoparticles exited from epithelia and entered into the lamina propria, as evidenced by the weak fluorescence signals in this region. The distribution pattern was different in level II~IV. Both epithelium and lamina propria showed high uptake of WGA-NP (Fig. 1b, c, d, f). This is because the level I is predominated by the presence of respiratory mucosa, while levels II~IV contain more olfactory mucosa. The olfactory cells in the olfactory mucosa are bipolar sensory neurons, projecting a dendrite to the surface of the nasal epithelium and a long axon toward the olfactory bulb, which is beneficial for transport of nanoparticles across the epithelium (9). Mucus-producing Bowman glands in the lamina propria (9) also showed high levels of WGA-NP fluorescence (Fig. 1b, c, f). Furthermore, green fluorescence was observed in the connective tissue around the olfactory nerve bundles passing through the cribriform plate (Fig. 1d, g, h). The data were consistent with the results shown by immunohistochemisty staining (Fig. 1 bottom). Green fluorescent nanoparticles were seen in glands, olfactory nerve bundles and the

connective tissues surrounding the olfactory nerve bundles (Fig. 1i, j). While in the cribriform plate region (level IV, Fig. 1k), only a small amount of nanoparticles was colocalized with nerve bundles, and others were distributed around it. These phenomena indicated that WGA-NP were absorbed into olfactory submucosa through olfactory cells, support cells, Bowman ducts and glands. After entering the lamina propria, WGA-NP were transferred into the olfactory nerve bundles or their surrounding connective tissue.

Selective Distribution of WGA-NP in Nasal Mucosa

Thirty minutes after intranasal instillation of 6-coumarin-loaded WGA-NP, strong green fluorescence was observed in the olfactory epithelium as well as in the connective tissues around the olfactory nerve bundles while much less green signals were detected in the respiratory epithelium (Fig. 1l, m). Our results agreed with Jansson and Björk (9), who visualized much more fluorescein dextran in the olfactory epithelium than in the respiratory epithelium after intranasal administration to rats. This may be attributed to the following three facts. First of all, WGA, specifically binding to *N*-acetylglucosamine and sialic acid, showed a greater binding affinity to the olfactory epithelium than to the respiratory one (19). Secondly, the olfactory epithelium contains a number of endocytic vesicles, exhibiting remarkably higher permeability than the respiratory epithelium (20). And thirdly, the cilia of the olfactory epithelium are static and the mucus in the olfactory mucosa is more viscous than that in the respiratory one (21), resulting in longer contact time of WGA-NP with the olfactory mucosa. Since olfactory mucosa plays a vital role in the transport of drugs into the brain and CSF (22), these results suggested that WGA-NP as a nanocarrier will help to enhance the brain delivery of drugs.

Transport Pathway Through Olfactory Epithelium

Drug absorption through the epithelium was mainly via two pathways: transcellular and paracellular pathway. There are tight junctions between the olfactory epithelial cells with the diameter less than 10A°, which are almost impermeable to molecules with a radius larger than 15A° (20,23). Because the particle size of WGA-NP is about 110 nm, paracellular transport of the nanoparticles seems unlikely. To demonstrate this speculation, ZO-1 peptide in tight junction between epithelial cells was stained with anti-ZO-1 antibody (red). As shown in Fig. 2, the olfactory mucosa had a high level of green fluorescence, indicating extensive uptake of WGA-NP. Almost all the red dots representing tight junction and green dots dedicated by nanoparticles were not colocalized, suggesting WGA-NP were primarily absorbed transcellularly through the olfactory epithelium.

Distribution of WGA-NP in Rat Olfactory Bulb

Following intranasal administration, the uptake of nanoparticles was rapid, as evidenced by the green fluorescence in the olfactory bulb at the initial time point, 5 min (Fig. 3 top a, e, h). Fluorescence signals of WGA-NP in olfactory bulb reached peak at 30 min following administration (Fig. 3 top b, f, i), but almost disappeared at 2 h. (Fig. 3 top c, g, j), indicating nanoparticles were cleared into blood or other tissues.

Five minutes after administration, green fluorescence was seen in the olfactory nerve layer, the glomerular layer, the external plexiform layer, mitral cell layer and granular cell layer in the olfactory bulb. However, no WGA-NP were observed in the innermost layers (a coronal section of olfactory bulb was presented in Fig. 3 bottom). Thirty minutes later, a high level of green fluorescence was visualized in glomerular layer and the external plexiform layer of the olfactory bulb. The granular cell layer also showed moderate level of WGA-NP fluorescence. Even Olfactory ventricle, located in the innermost side of olfactory bulb, showed weak fluorescence, implying nanoparticles were transported from outside into inside of olfactory bulb. Since the olfactory nerve bundles terminate in the glomerular layer of the olfactory bulb, high green fluorescence observed in glomerular layer suggested that a proportion of WGA-NP were transported to the brain via olfactory pathway.

Two pathways were proposed for the transfer of substances via olfactory pathway: olfactory nerve pathway and olfactory epithelial pathway (6). The transneuronal transport has been

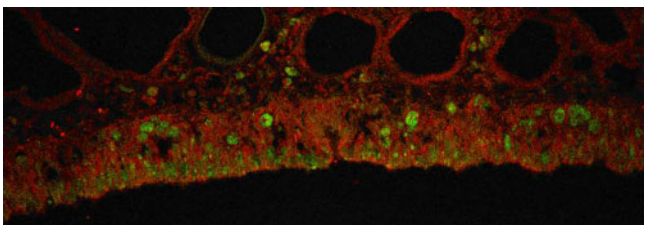

Fig. 2 Representative fluorescence micrographs for the olfactory mucosa from rats ($n=3$) 5 min after intranasal administration of WGA-NP (*green*). ZO-1 peptide in tight junction was stained with anti-ZO-1 antibody (*red*) to visualize the cell borders. Non-colocalization of tight junction (*red*) and nanoparticles (*green*) suggested that WGA-NP were primarily absorbed transcellularly through the olfactory epithelium.

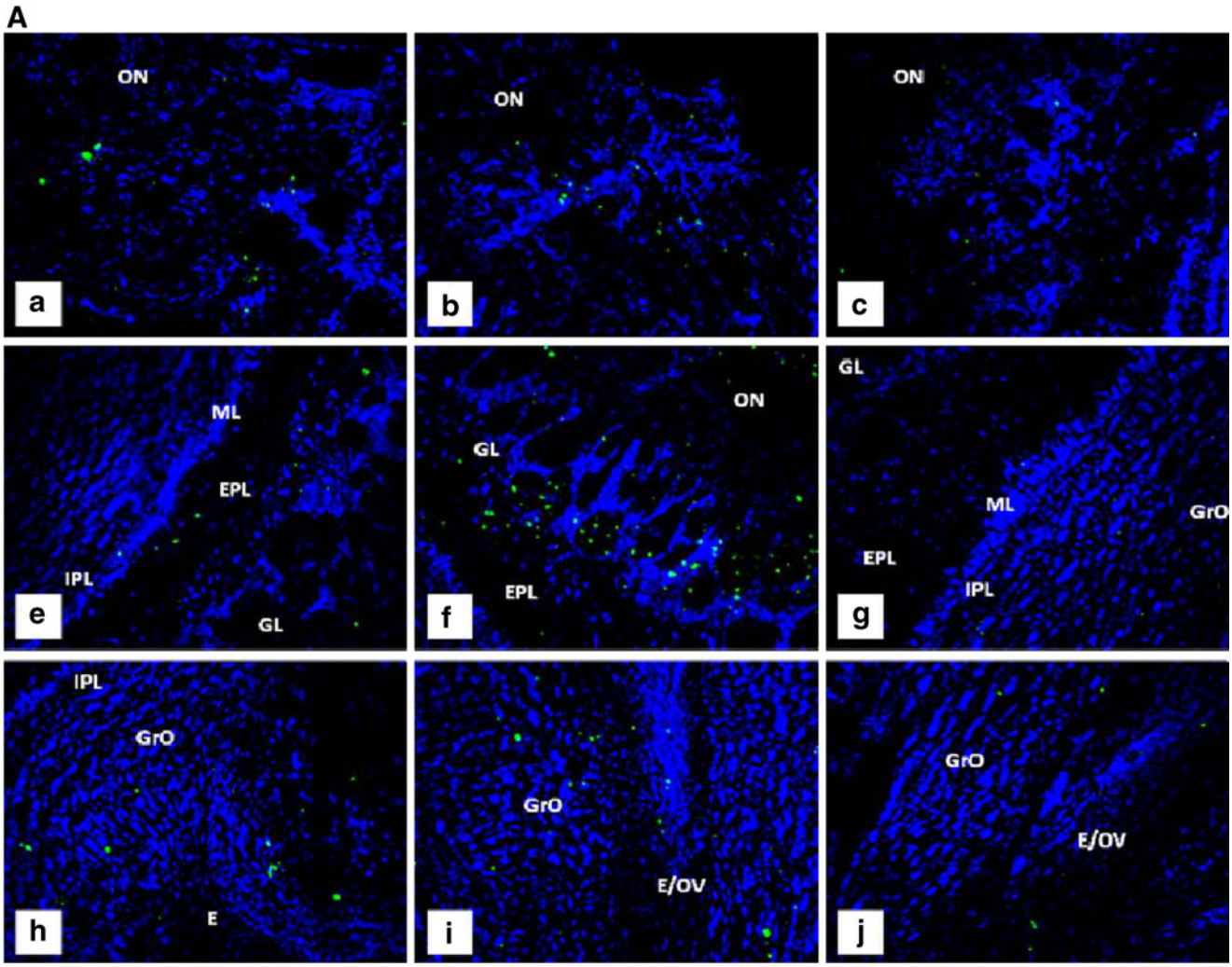

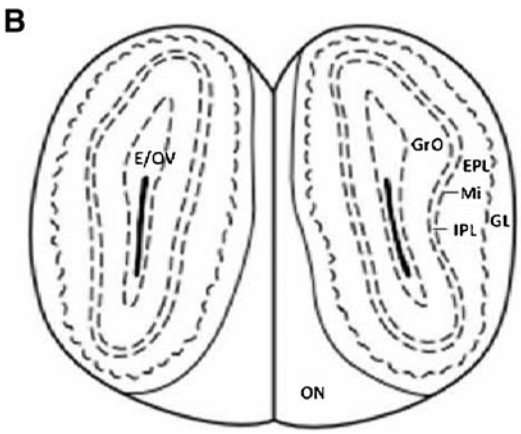

Fig. 3 (**A**) Distribution of WGA-NP (green) in rat olfactory bulb (n=3) at 5 min (**a**, **e**, **h**), 30 min (**b**, **f**, **i**) and 120 min (**c**, **g**, **j**). Cell nucleus stained with DAPI (*blue*) (100×). (**B**) Drawing of a coronal section at the location of olfactory bulb. Fluorescence signals of WGA-NP in the olfactory bulb were observed within 5 min and reached peak at 30 min. A high level of green fluorescence was visualized at 30 min in glomerular layer in which the olfactory nerve bundles terminate, suggesting that a proportion of WGA-NP were transported to the brain via olfactory pathway. ON: Olfactory nerve layer; GL: Glomerular layer; EPL: external plexiform layer; Mi: Mitral cell layer; GrO: granular cell layer; IPL: internal plexiform; E: ependyma and subependymal layer; OV: Olfactory ventricle.

demonstrated to be very slow, with substances reaching the brain as late as 24 h after dosing (24). On the contrary, the olfactory epithelial pathway that involves transcellular transport across the epithelium or paracellular diffusion through the tight junctions is considered to be quick (1), which possibly accounts for the rapid appearances of several drug molecules in CSF and brain such as dihydroergotamine (24), lidocaine (25) and cocaine (26). The olfactory ensheathing cells surrounding the olfactory axons produce continuous conduits, which are kept open regardless of degeneration or regeneration of the olfactory neurons. Nanoparticles might enter into the conduits surrounding the olfactory nerve bundles instead of intra-bundles and then transfer into the olfactory bulb. In the present study, WGA-NP were observed in the olfactory bulb at 5 min after administration, indicating that WGA-NP were transferred into the olfactory bulb most possibly via olfactory epithelial pathway.

Distribution of WGA-NP in the Brain

Distribution of ^{125}I-WGA-NP following intranasal administration was measured in SD rats and the levels of radioactivity in blood, lymph nodes, trigeminal nerve, cerebrospinal fluid (CSF) and brain tissues are shown in Table I. Nasal absorption of nanoparticles into the systemic circulation was rapid, and the plasma level remained almost constant until 2 h post application.

It was reported that after intranasal administration, nanoparticles might be uptaken by M cells of the nasal-associated lymphoid tissue (NALT) (27) and then concentrated in the lymph nodes. Moreover, the deep and superficial cervical lymph nodes receive afferent lymphatic drainage from the nasal cavity and nasolabial region, respectively (10). Therefore, the radioactivity of nanoparticles in several lymph nodes was determined. At 5 min after intranasal administration, the deep cervical lymph nodes showed high levels of radioactivity, which was 10.4 times as high as that in the olfactory bulb. However, superficial cervical or axillary lymph nodes, especially the latter, which do not receive lymphatic drainage from the nasal lymphatic vessel, exhibited significant lower levels of radioactivity than that in the deep cervical lymph nodes 5 min after intranasal administration of ^{125}I-WGA-NP. Two hours later, almost same radioactivity was found in the three lymph nodes, which is most likely a result of lymph circulation.

Five minutes after intranasal administration of ^{125}I-WGA-NP, different concentrations of radioactivity were observed around CNS areas, with levels decreasing in the rostral-

Table I Amount-Time Profiles of Radioactivity in the Blood, CNS, Trigeminal Nerve and Lymphatic Tissue Following Intranasal Administration of ^{125}I-WGA-NP

Tissue	Amount of ^{125}I-WGA-NP in tissue (cpm/g tissue/g dose × 100,%)		
	5 min	30 min	120 min
Blood	10.69 ± 3.16	12.11 ± 3.16	12.26 ± 2.17
CNS			
Olfactory bulb	3.49 ± 1.01[a]	10.88 ± 6.95[b]	1.31 ± 0.80
Ant. olfactory nucleus	1.76 ± 0.76[a]	4.27 ± 2.39[b]	1.21 ± 0.67
Frontal cortex	1.30 ± 0.75	1.37 ± 0.80	0.76 ± 0.35[a]
Motor cortex	0.89 ± 0.49	0.74 ± 0.29[a]	0.64 ± 0.18
Caudate putamen (Striatum)	0.72 ± 0.68	0.59 ± 0.26	0.35 ± 0.22[a]
Hippocampal formation	0.52 ± 0.11	0.68 ± 0.29	0.45 ± 0.16
Diencephalon	0.62 ± 0.23	0.80 ± 0.25	0.50 ± 0.17
Midbrain	0.67 ± 0.16	0.74 ± 0.40	0.48 ± 0.18
Cerebellum	0.68 ± 0.16	1.43 ± 0.87[a]	0.71 ± 0.38
Pons	0.84 ± 0.31	1.15 ± 0.49	0.49 ± 0.20
Medulla	1.53 ± 0.96	1.69 ± 0.70[b]	0.72 ± 0.54
Cervical spinal cord	2.25 ± 2.55	5.39 ± 4.47[a]	0.86 ± 0.41
Cerebrospinal fluid	0.61 ± 0.29	0.55 ± 0.57[a]	0.55 ± 0.28[b]
Trigeminal nerve	128.41 ± 64.01[b]	140.52 ± 47.66[a]	9.52 ± 5.64[a]
Lymph nodes			
Deep cervical lymph nodes	36.42 ± 23.22	30.66 ± 17.54[a]	5.62 ± 2.36
Superficial cervical lymph nodes	4.02 ± 3.24[b]	5.97 ± 2.04	4.45 ± 1.03[b]
Axillary lymph nodes	2.84 ± 0.89[a]	5.40 ± 1.09[a]	4.95 ± 0.92[b]

Data are represented as mean ± SD (n=6 unless indicated otherwise; a: n=5; b: n=4)

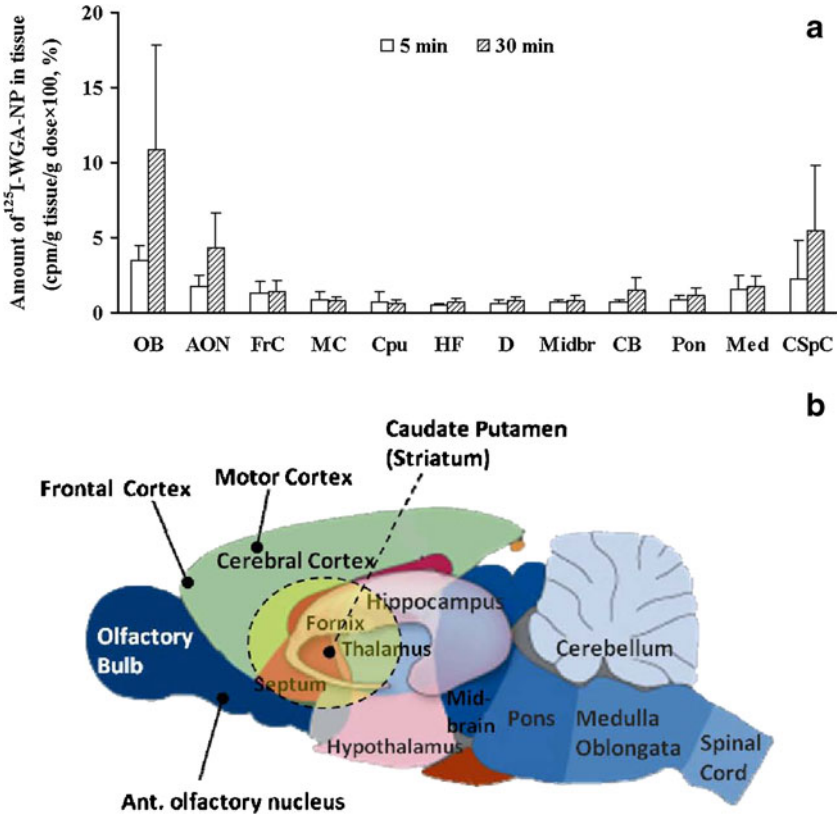

Fig. 4 (**a**) Distribution of ^{125}I-WGA-NP in olfactory bulb (OB), anterior olfactory nucleus (AON), frontal cortex (FrC), motor cortex (MC), caudate putamen (CPu), hippocampal formation (HF), diencephalon (D), midbrain (Midbr), cerebellum (CB), pons (Pon), medulla (Med) and cervical spinal cord (CSpC) following intranasal administration after 5 min and 30 min (n=4–6). (**b**) Illustration of rat brain structure.

to-caudal direction from the olfactory bulb (e.g. olfactory bulb > anterior olfactory nucleus > frontal cortex > motor cortex > striatum > hippocampus) and in the caudal-to-rostral direction from the caudal cervical spinal cord (e.g. cervical spinal cord > medulla > pons > cerebellum, Fig. 4). The trigeminal nerve showed significantly higher radioactivity than any other tissues and a 38.6-fold radioactivity than the olfactory bulb (Table I). Thirty minutes post application, nanoparticles concentrations in olfactory bulb and trigeminal nerve increased further, with the concentration in its neighboring tissues such as anterior olfactory nucleus (next to olfactory bulb), cervical spinal cord and medulla (axons of the trigeminal nerve extend to cervical spinal cord and medulla) increasing. Two hours later, the radioactivity in all sampled brain tissues was kept at a lower level.

Although several therapeutics have been reported to directly reach the CSF following nasal instillation (28,29), in the present study, low radioactivity was detected in CSF (similar to that in diencephalons and hippocampus, far below that in olfactory bulb and trigeminal nerve). This result is consistent with our pharmacokinetic study that CSF contained very low 6-coumarin content after intranasal administration of 6-coumarin-loaded WGA-NP (data not shown). Thorne *et al.* (10) also found that no radioactivity was detected in the CSF even though the rats were intranasally given relatively high doses of ^{125}I-IGF-1.

The brain transfer of WGA-NP was also visualized by the near infrared fluorescence probe image at 5–120 min after intranasal administration. The fluorescent intensity in whole brain, olfactory bulb and trigeminal nerve of both WGA-NP and NP reached maximum at 30 min and then decreased at 120 min (Fi5. 6A, B, C). There was a significantly accumulated amount of WGA-NP in these tissues compared with that of NP following intranasal administration, suggesting that WGA modification enhanced nanoparticles delivery to the brain, which is consistent with our previous reports (5,14).

The fluorescence signal of WGA-NP appeared in the anterior olfactory nucleus, pons and medulla oblongata as early as 5 min after intranasal administration. At 30 min, stronger fluorescence signals were observed in the whole area of brain sections and the signals became weak at 120 min (Fig. 5d, sagittal slices), implying nanoparticles entering into olfactory bulb and trigeminal nerve were further transferred to neighboring brain tissues and diffused in whole brain. Similar phenomena were observed in unmodified NP (Fig. 5d).

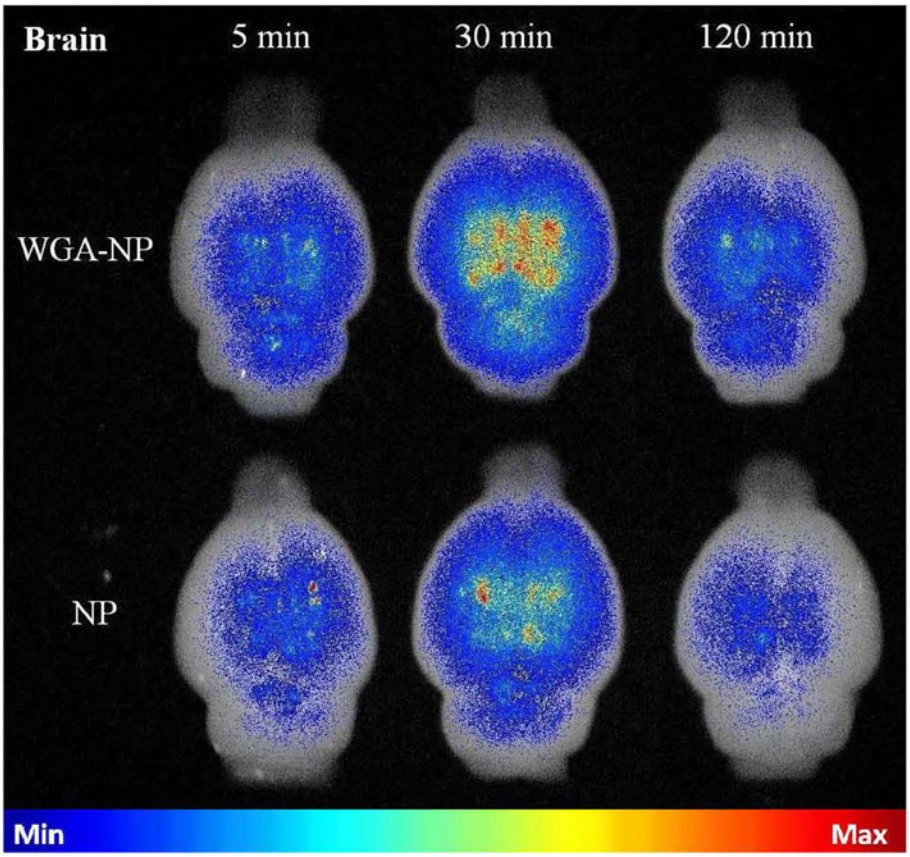
Brain
5 min
30 min
120 min
WGA-NP
NP
Min
Max

a

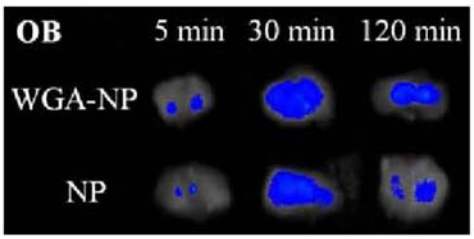
OB
5 min
30 min
120 min
WGA-NP
NP

b

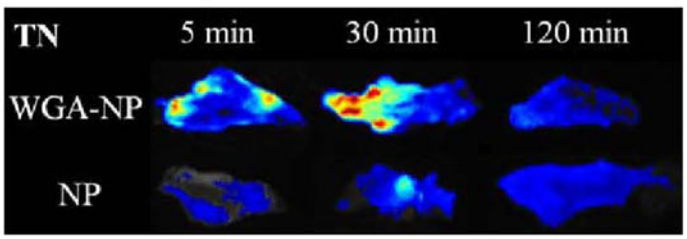
TN
5 min
30 min
120 min
WGA-NP
NP

c

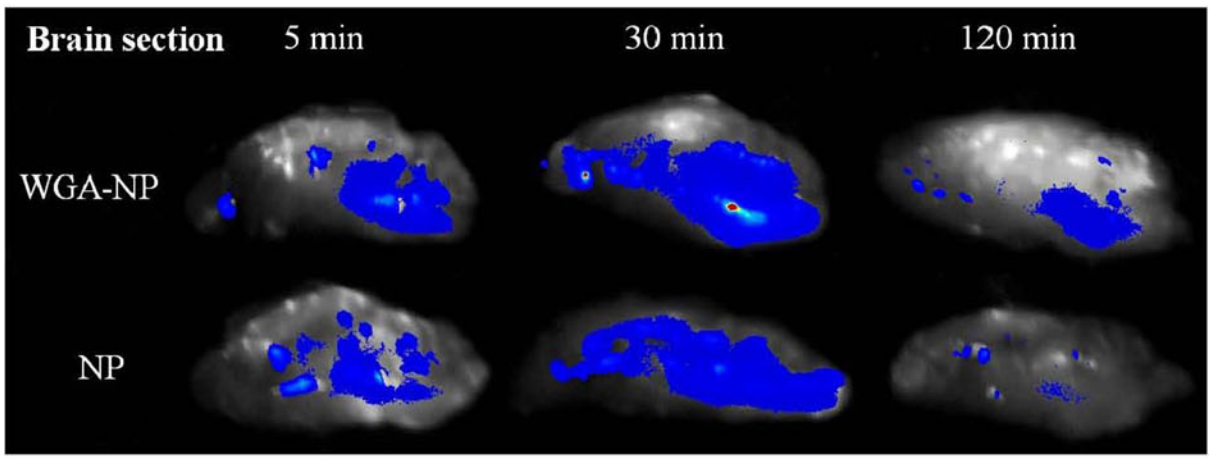
Brain section
5 min
30 min
120 min
WGA-NP
NP

d

◀ **Fig. 5** Near-IR fluorescence images of brain (**a**), OB (**b**), TN (**c**) and midsagittal sections of brain (**d**) 5 min, 30 min and 120 min after intranasal administration of NP and WGA-NP under CRi Mastreo small animals imaging system. Fluorescence signals of nanoparticles appeared in the olfactory bulb, anterior olfactory nucleus, pons, medulla oblongata and trigeminal nerve as early as 5 min and became stronger at 30 min, indicating that both NP and WGA-NP were transported to the brain via olfactory pathway and trigeminal nerve pathway. OB: olfactory bulb, TN: trigeminal nerve.

The potential pathways for WGA-NP transport to the brain may be illustrated (Fig. 6) and summed up as follows:

1) Olfactory pathway: Olfactory pathway has been reported as a major component of intranasal administration to deliver therapeutics directly into the CNS. The nasal barrier to the brain might be "leaky" because the olfactory cells regenerate every 3–4 weeks due to exposure to external toxins (30,31). In addition, the continuous perineurial channels generated by the olfactory ensheathing cells that envelop the axons of olfactory cells are kept open (32). As a result, intranasally administered WGA-NP may reach the brain via extracellular transport along olfactory nerves. Further, neural projections of the olfactory bulb extend into multiple rostral brain tissues such as the olfactory tract, anterior olfactory nucleus, piriform cortex and so on (33). Therefore, the significant WGA-NP distribution in rostral brain areas neighboring from the olfactory bulb is mainly due to the olfactory pathway.
2) Trigeminal nerve pathway: The trigeminal nerve enters the brainstem at the pons and some of its nerve endings terminate beneath the nasal epithelial surface (1,34), which provides possible entrance for intranasally administrated WGA-NP into the brain. In this study, high concentrations of WGA-NP were detected in the cervical spinal cord and medulla, demonstrating the involvement of the trigeminal nerves. The diameter of trigeminal nerve endings is about 0.2~1.5 μm (35), while WGA-NP has a particle size smaller than 0.2 μm, so nanoparticles might be transported along trigeminal nerve via intracellular mechanisms (propelled by axonal flow). Nevertheless, considering the rapid delivery with high radioactivity in cervical spinal cord determined 5 min after intranasal administration, extracellular mechanism is most likely to be the predominant mode of transport into the CNS via the trigeminal nerve pathway.
3) CSF pathway: The CSF pathway is considered to be an important way of delivering intranasally administrated drugs to the CSF and brain because it connects the subarachnoid space containing CSF, perineurial spaces surrounding olfactory nerves and the nasal lymphatics (1,36). However, CSF did not exhibit high radioactivity at the three time points post administration, suggesting that the CSF pathway just plays a limited role in brain transport of intranasally administered WGA-NP.

Similarly, the olfactory pathway and the trigeminal nerve pathway are involved in the delivery of unmodified NP from nose to brain (Fig. 5). Although modification of nanoparticles with WGA can enhance the amount of nanoparticles delivery from nose to brain as evidenced by *in vivo* studies (5,14), it has no significant effect on the transport pathways of nanoaprticles.

Generally, neurological diseases occur in some specific regions of the brain, which requires efficient drug delivery not only to the brain but also to these specific regions. For example, Alzheimer's disease (AD), a neurodegenerative disease afflicting ~35 million people worldwide in 2009 (37), has been demonstrated to damage cerebral cortex and hippocampus, two areas near to the olfactory bulb (see Fig. 4 bottom). Therefore, for the treatment of AD, drug delivery system designed to target the olfactory mucosa such as WGA-NP, which has high affinity to the olfactory epithelium, may be rational. Similarly, drug delivery system designed to target the trigeminal nerve may be beneficial to deliver therapeutics for the treatment of the brain diseases in caudal region such as cerebellar atrophy. Our findings may provide valuable information for the rational design of nanocarriers to improve the treatment of neurological and psychiatric diseases.

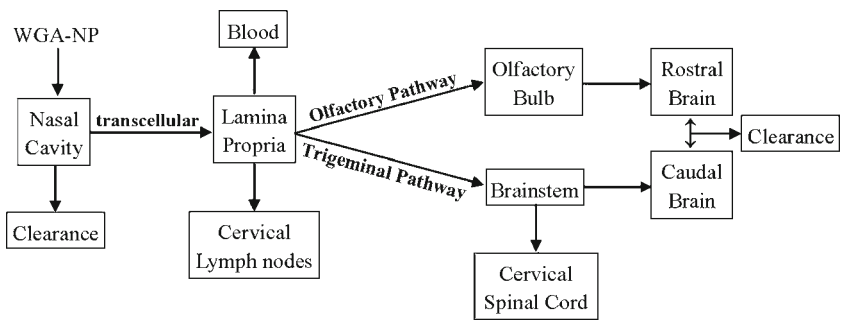

Fig. 6 Schematic diagram of WGA-NP transport from nose to the brain. After intranasal administration, WGA-NP enter the lamina propria transcellularly and are further transported to the brain via olfactory pathway and trigeminal nerve pathway.

CONCLUSIONS

In the present study, we explored the nose-to-brain transport pathways of WGA-NP using histotomy, radiation isotope labeling and *ex vivo* imaging method. The results showed that WGA-NP are mainly transported to the CNS via extracellular mechanism along olfactory nerves and trigeminal nerves in 2 h following intranasal administration. CSF pathway has little contribution to the transport process. Given the short experimental period in this work, further investigation about nanoparticle transport in longer time, for example 24 h, may be needed to make sure whether nanoparticles can be transferred along trigeminal nerves via intracellular mechanisms.

ACKNOWLEDGMENTS & DISCLOSURES

This work was supported by National Natural Science Foundation of China (No.30772657), National Basic Research Program of China (No. 2007CB935802), and National Science and Technology Major Project (2009ZX09310-006).

REFERENCES

1. Dhuria SV, Hanson LR, Frey 2nd WH. Intranasal delivery to the central nervous system: mechanisms and experimental considerations. J Pharm Sci. 2010;99(4):1654–73.
2. Graff CL, Pollack GM. Nasal drug administration: potential for targeted central nervous system delivery. J Pharm Sci. 2005;94 (6):1187–95.
3. Kim TW, Chung H, Kwon IC, Sung HC, Jeong SY. *In vivo* gene transfer to the mouse nasal cavity mucosa using a stable cationic lipid emulsion. Mol Cells. 2000;10(2):142–7.
4. Dufes C, Olivier JC, Gaillard F, Gaillard A, Couet W, Muller JM. Brain delivery of vasoactive intestinal peptide (VIP) following nasal administration to rats. Int J Pharm. 2003;255(1–2):87–97.
5. Gao X, Wu B, Zhang Q, Chen J, Zhu J, Zhang W, Rong Z, Chen H, Jiang X. Brain delivery of vasoactive intestinal peptide enhanced with the nanoparticles conjugated with wheat germ agglutinin following intranasal administration. J Control Release. 2007;121 (3):156–67.
6. Mathison S, Nagilla R, Kompella UB. Nasal route for direct delivery of solutes to the central nervous system: fact or fiction? J Drug Target. 1998;5(6):415–41.
7. Faker WF. The nasal mucosa and the subarachnoid space. Am J Anat. 1937;62(1):121–48.
8. Rake G. The rapid invasion of the body through the olfactory mucosa. J Exp Med. 1937;65(2):303–15.
9. Jansson B, Bjork E. Visualization of *in vivo* olfactory uptake and transfer using fluorescein dextran. J Drug Target. 2002;10 (5):379–86.
10. Thorne RG, Pronk GJ, Padmanabhan V, Frey 2nd WH. Delivery of insulin-like growth factor-I to the rat brain and spinal cord along olfactory and trigeminal pathways following intranasal administration. Neuroscience. 2004;127(2):481–96.
11. Thorne RG, Hanson LR, Ross TM, Tung D, Frey II WH. Delivery of interferon-b to the monkey nervous system following intranasal administration. Neuroscience. 2008;152(3):785–97.
12. Banks WA, Broadwell RD. Blood to brain and brain to blood passage of native horseradish peroxidase, wheat germ agglutinin, and albumin: pharmacokinetic and morphological assessments. J Neurochem. 1994;62(6):2404–19.
13. Panyam J, Labhasetwar V. Dynamics of endocytosis and exocytosis of poly(d, l-lactide -co-glycolide) nanoparticles in vascular smooth muscle cells. Pharm Res. 2003;20(2):212–20.
14. Gao X, Tao W, Lu W, Zhang Q, Zhang Y, Jiang X, Fu S. Lectin-conjugated PEG-PLA nanoparticles: preparation and brain delivery after intranasal administration. Biomaterials. 2006;27(18):3482–90.
15. Ohtake K, Maeno T, Ueda H, Natsume H, Morimoto Y. Poly-l-arginine predominantly increases the paracellular permeability of hydrophilic macromolecules across rabbit nasal epithelium *in vitro*. Pharm Res. 2003;20(2):153–60.
16. Qian J, Tang X, Wan DJ, Zhu JH. Radioisotopic tracing method of hirulog-like peptide. Chem J Chin Univ. 2006;27 (7):1247–9.
17. Raghuramulu N, Rao BS. Stability of ^{125}I-labeled insulin used in radioimmunoassay of insulin. J Nucl Med. 1972;13(8):621–3.
18. Dahlin M, Björk E. Nasal absorption of (S)-UH-301 and its transport into the cerebrospinal fluid of rats. Int J Pharm. 2000;195(1–2):197–205.
19. Takami S, Getchell ML, Getchell TV. Lectin histochemical localization of galactose, N-acetylgalactosamine, and *N*-acetyl-glucosamine in glycoconjugates of the rat vomeronasal organ, with comparison to the olfactory and septal mucosa. Cell Tissue Res. 1994;277(2):211–30.
20. Bannister LH, Dodson HC. Endocytic pathways in the olfactory and vomeronasal epithelia of the mouse: Ultrastructure and uptake of tracers. Microsc Res Tech. 1992;23(2):128–41.
21. Uraih LC, Maronpot RR. Normal histology of the nasal cavity and application of special techniques. Environ Health Prespect. 1990;85:187–208.
22. Illum L. Transport of drugs from the nasal cavity to the central nervous system. Eur J Pharm Sci. 2000;11(1):1–18.
23. Madara JL, Dharmsathaphorn K. Occluding junction structure function relationship in a cultured epithelial monolayer. J Cell Biol. 1985;101(6):2124–33.
24. Wang Y, Aun R, Tse FLS. Brain uptake of dihydroergotamine after intravenous and nasal administration in the rat. Biopharm Drug Dispos. 1998;19(9):571–5.
25. Chou KJ, Donovan MD. The distribution of local anesthetics into the CSF following intranasal administration. Int J Pharm. 1998;168(2):137–45.
26. Chow HHS, Chen Z, Matsuura GT. Direct transport of cocaine from the nasal cavity to the brain following intranasal cocaine administration in rats. J Pharm Sci. 1999;88 (8):754–8.
27. Tobío M, Gref R, Sánchez A, Langer R, Alonso MJ. Stealth PLA-PEG nanoparticles as protein carriers for nasal administration. Pharm Res. 1998;15(2):270–5.
28. Born J, Lange T, Kern W, McGregor GP, Bickel U, Fehm HL. Sniffing neuropeptides: a transnasal approach to the human brain. Nat Neurosci. 2002;5(6):514–6.
29. Wang Q, Chen G, Zeng S. Pharmacokinetics of Gastrodin in rat plasma and CSF after i.n. and i.v. Int J Pharm. 2007;341 (1–2):20–5.
30. Mackay-Sim A. Neurogenesis in the adult olfactory neuroepithelium. In: Doty RL, editor. Handbook of olfaction and gustation. 2nd ed. New York: Marcel Dekker; 2003. p. 93–113.
31. Balin BJ, Broadwell RD, Salcman M, el-Kalliny M. Avenues for entry of peripherally administered protein to the central nervous system in mouse, rat, and squirrel monkey. J Comp Neurol. 1986;251(2):260–80.

32. Williams SK, Franklin RJ, Barnett SC. Response of olfactory ensheathing cells to the degeneration and regeneration of the peripheral olfactory system and the involvement of the neuregulins. J Comp Neurol. 2004;470(1):50–62.
33. Buck LB. The chemical senses. In: Kandel ER, Schwartz JH, Jessell TM, editors. Principles of neural science. 4th ed. New York: McGraw-Hill Companies; 2000. p. 625–52.
34. Silver WL. The common chemical sense. In: Finger TE, Silver WL, editors. Neurobiology of taste and smell. Malabar: Krieger; 1991. p. 65–87.
35. Alimohammadi H, Silver WL. Evidence for nicotinic acetylcholine receptors on nasal trigeminal nerve endings of the rat. Chem Senses. 2000;25(1):61–6.
36. Boulton M, Young A, Hay J, Armstrong D, Fless-ner M, Schwartz M, Johnston M. Drainage of CSF through lymphatic pathways and arachnoid villi in sheep: measurement of ^{125}I-albumin clearance. Neuropathol Appl Neurobiol. 1996;22(4):325–33.
37. Cushman M, Johnson BS, King OD, Gitler AD, Shorter J. Prion-like disorders: blurring the divide between transmissibility and infectivity. J Cell Sci. 2010;123(pt 8):1191–201.